FATIGUE LIFETIME OF BEARING STEEL IN ULTRA-HIGH-CYCLE REGION

L. Kunz and P. Lukáš
Institute of Physics of Materials, ASCR, 616 62 Brno, Czech Republic
M. Činčala
University of Žilina, 01026 Žilina, Slovak Republic
G. Nicoletto
University of Parma, 43100 Parma, Italy

ABSTRACT

Experimental fatigue lifetime data in ultra-high-cycle region have been shown to exhibit sometimes a "two-stage", "stepwise" or "duplex" S-N curves. The majority of these observations have been performed on high strength bearing steels using rotating bending loading. It has been pointed out that this effect is related to different types of crack initiation in low-cycle and ultra-high-cycle regions. Recently, some authors expressed the opinion that the two-stage S-N curves are related rather to the type of loading than to the material and the type of fatigue crack initiation.
In order to contribute to the elucidation of this problem, a direct comparison of S-N curves of bearing steel determined in uniaxial tension-compression and rotating bending was performed. An obvious difference in the S-N curve shape was observed. Continuously increasing number of cycles to fracture with decreasing stress amplitude characterizes the tension-compression S-N data, whereas pronounced two-step curve is characteristic of rotating bending tests. It has been shown that the rotating bending S-N data fit the tension-compression ones when the correction in terms of local stress amplitude at the crack initiation site is applied.

Introduction

Fatigue behaviour of materials under cyclic loading in high-cycle and ultra-high-cycle regions is a topic of increasing importance due to rising demands on lifetime of engineering components. High-speed trains, car engines, turbines and pressure vessels are typical examples of engineering structures exposed to number of loading cycles exceeding 10^9 [1]. The engineering requirement of safe design in ultra-high-cycle region (up to 10^{11}cycles) reflects e.g. ASME boiler and pressure vessel code [2]. The conventional S-N curve, defined in reference to carbon steels, is usually limited by 10^7 cycles. It is admitted that the horizontal line determines the fatigue limit characterizing the infinite life. Contrary to this, fatigue fracture of high-strength steels has been observed after considerably higher number of cycles than 10^7, namely in the region of 10^8 to 10^{10}. Consequently, the fatigue limit defined on the basis of 10^7 cycles cannot guarantee a safe design for high strength bearing steels, which are exposed typically to the number of loading cycles in gigacycle region.

Presentation of constant amplitude fatigue test results for low-cycle and high-cycle fatigue is described by standards, e.g. ASTM E468. The test results may be expressed by two straight lines in logarithmic co-ordinates, one of which is horizontal line representing the fatigue limit, the second is a hyperbola asymptotic to fatigue limit or a more general curvilinear relation. Experimental studies performed on high strength steels provided strong evidence that the S-N diagrams exhibit more complicated shape for loading exceeding 10^7 cycles, e.g. [3 - 8]. The S-N curves exhibit a plateau usually in the range of 10^5 to 10^7 cycles. Further increase of number of cycles to fracture with decreasing amplitude is observed in ultra-high-cycle region with the tendency to reach the second lower fatigue limit. The S-N curves are described as "two-stage", "stepwise" or as "duplex" composed from two different S-N curves. Particular parts has been shown to correlate closely either with the surface crack initiation or internal crack initiation. The origins of surface crack initiation are cyclic slip activity, inclusions or eventually defects made by drop off inclusions by surface treatment of specimens. It is implicitly taken for granted that defects of specimen surface in form of scratches, artificial impressions and roughness causing stress concentration are removed by careful surface preparation. Surface crack initiation is characteristic for fatigue fractures, which appear before the number of cycles of the order of 10^6 is reached. Internal crack initiation is generally related to material inhomogeneities and was reported at a number of cycles to fracture up to the order of 10^9. The internal crack initiation can be studied only indirectly, usually after the final fracture.

It has been shown, that there are several mechanisms, which may cause or influence fatigue failure in ultra-high-cycle region. The effect of internal hydrogen trapped by non-metallic inclusions resulting in particular fracture surface morphology near non-metallic inclusions called optically dark area has been discussed in [9, 10]. The possible influence of specific strain concentration at the suitable oriented internal grain boundaries or at small precipitates, inclusions or very small grains lodged between two or three large grains was analysed in [11]. Mughrabi [12, 13] theoretically predicted a “two step” fatigue life diagram even for pure ductile metals and alloys, which do not contain inclusions. The plateau at the fatigue life diagram is explained by the existence of plastic strain fatigue limit. It is assumed that it may be terminated in the ultra-high-cycle region by the transition to a threshold of negligible cyclic slip irreversibility. The life controlling mechanism is considered to be crack initiation resulting from surface roughening, subsequent cyclic strain localization and very slow stage I crack growth.

The majority of the experimental determination of two-stage S-N diagrams has been performed on high strength steels using rotating bending test [3, 5, 8, 14 –21]. Recently Marines et al. [22] published S-N data in tension-compression at frequencies of 35 Hz, 20 and 30 kHz. Continuously decreasing dependence from the mega to gigacycle region was found. Their results indicate that the two-stage curve is more related to the rotating bending loading than the steel itself. Sakai et al. [6] using push-pull axial loading and 50 Hz frequency found duplex S-N curve. From comparison of this result with data for the same kind of steel loaded in rotating bending authors conclude that the plateau or the stepwise character of S-N dependence is more pronounced for rotating bending than for axial loading. Apparent two-stage curve was observed by Wang and co-workers [7, 23] for 20 kHz push-pull loading. Contrary to this Murakami et al. [9] found a continuously decreasing S-N curve of a high strength steel SCM435 loaded in tension-compression with the stress ratio R = – 1 at frequencies 30-100Hz.

Papers by Murakami et al. [10], Mughrabi [13] and Marines et al. [22] indicate that the aspects of the two-stage S-N curves have to be discussed in terms of experimental methods used, specimen size and distribution of inclusion size. The large scatter of experimental data, characteristic for high strength steels, can be significantly reduced taking into account the defect size [9]. Analysis of fatigue crack initiation location resulting in correction of stress amplitude for rotating bending test and comparison with tension-compression data performed in [22] results in the claim that the two-step S-N curve can be transformed to a continuously decreasing curve approaching a true fatigue limit in the gigacycle region.

The aim of this work was to perform a direct comparison of S-N curves of high strength bearing steel loaded in symmetrical tension-compression and rotating bending because none of the existing studies, to the authors’ knowledge, discusses fully comparable sets of data.

Material and Experimental

A bearing steel according to the Czech Standard ČSN 41 4109 (corresponding to the 100Cr6, ASTM E 52100 or JIS SUJ2 steels) with chemical composition as given in Tab. 1 has been used. The steel was delivered in bars after soft annealing.

Tab.1. Chemical composition of 100Cr steel, wt.%.

C	Mn	Si	Cr	Ni	Cu	P	S	Al	Ti	V	Zn	Zr	Mo	Co
1.0	0.34	0.28	1.48	0.10	0.12	0.01	0.01	0.009	0.163	0.033	0.09	0.018	0.009	0.021

Two types of specimens according to Fig.1 were used for fatigue tests. The specimens were machined with minimum working allowance of 0.8 mm. Following heat treatment of specimens consisted of an austenitization at 1113K for 20 min. followed by rapid quenching into oil. The resulting martensitic structure was annealed by stress relieving at 443 K with holding time of 90 min. followed by air-cooling. Heat-treated specimens were ground to the final shape. The minimum thickness of removed surface layer at the gauge length was 0.8 mm. The final manufacturing operation was very fine grinding of the gauge length by metallographic emery papers on a turn bench (tension-compression specimens) or by 6μm diamond spray (rotating bending specimens).

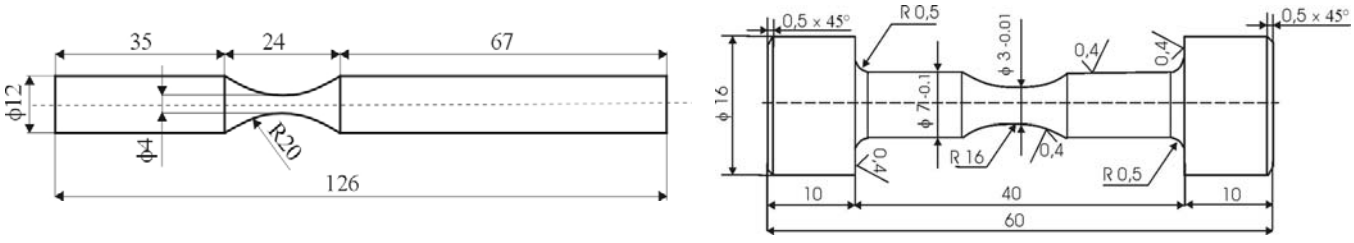

a) b)

Figure 1. Specimens for lifetime determination. a) rotating bending, b) tension compression.

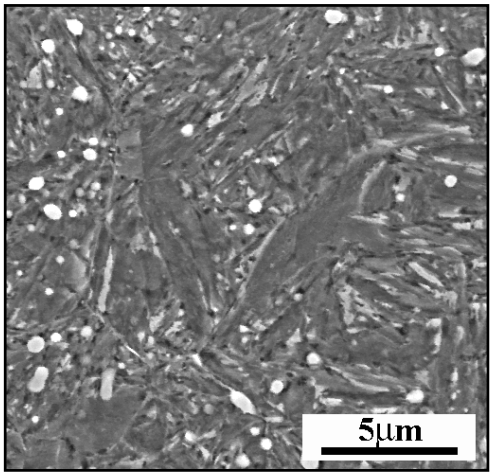

Figure 2. Microstructure of the steel studied.

The microstructure of the steel studied can bee seen in Fig.2. Regularly distributed carbides are embedded in a tempered martensite matrix. A residual austenite content of 6.4 ± 0.9 wt% was determined by diffractometric analysis. The hardness measured at the specimen cross-section varies between 650 and 713 HV.

Fatigue tests in tension-compression were conducted on a resonant machine Amsler under controlled load. The frequency of cycling was 190 Hz and the load wave was of sine type. The stress ratio R defined as ratio of minimum to maximum stress in a cycle was R_σ = -1. Fatigue tests were run at the room temperature in the ambient laboratory air. No heating of specimens was observed for the stress amplitudes used.

Fatigue tests in rotating bending were accomplished at the frequency of 50 Hz on a rotating bending testing machine Rotoflex at ambient laboratory temperature, air and humidity.

The tests were run either up to the final fracture of specimens or up to minimum number of cycles of the order of 10^8.

Detailed fractographic observation of all fracture surfaces was performed by means of scanning electron microscope JEOL 6460.

Results

Experimentally determined S-N data are shown in Figs 3a and 3b. Results of stress symmetrical loading in tension-compression can be seen in Fig. 3a. The experimental values exhibit a considerable scatter in the interval of 10^6 to 10^8 cycles, where the plateau on S-N curves has been usually reported. The distribution of experimental points does not support a two-stage curve. An inclined straight line can apparently make the best fit. On the other hand, S-N data determined in rotating bending on the same material can be best fitted by a two-stage curve with a clear plateau in the interval of 10^6 to 10^8 cycles, Fig. 3b.

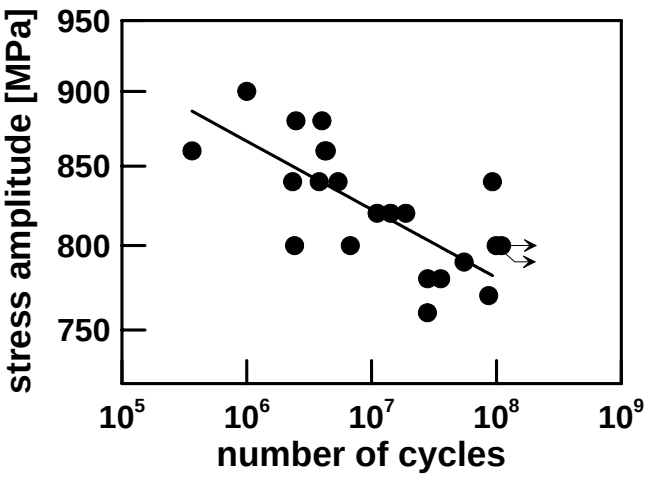

Figure 3a. S-N curve, tension-compression loading.

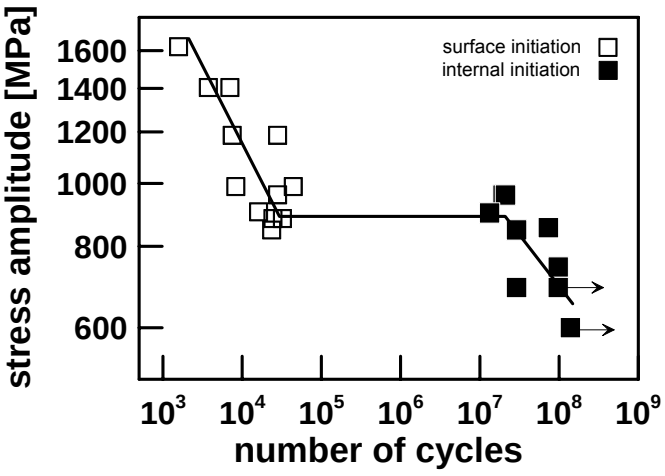

Figure 3b. S-N curve, rotating bending loading.

Fractographic analysis of fatigue fracture surfaces revealed that all specimens loaded in tension compression failed by fatigue fracture originating in material interior. From a mesoscopic point of view the fracture surfaces exhibit the typical fish eye appearance usually with an inclusion in fish eye centre. In 5 cases from the total number of 19 fractured specimens it was not possible to identify the inclusion at the initiation site, though both matching fracture surfaces were examined very carefully. Two types of inclusions were observed at the initiation site. An example of a large aluminium oxide inclusion can be seen in Fig.4. The inclusion contains nearly 42 wt. % of Al, 53 % of O and the rest is Fe, Cr and C (determined by X-ray diffractometric analysis). Decohesion of the inclusion/matrix interface is clearly visible. Steps on the fracture surface in the nearest vicinity of

the inclusion and fracture surface markings indicate the multiple fatigue crack initiation at the inclusion. Crack initiation at aluminium oxides was relatively rare. The most frequent type of internal fatigue crack initiation was related to small TiN inclusions. An example can be seen in Fig.5. The chemical composition of the inclusion shown in Fig.5 was 66% Ti, 19 % N, 9 % Cr and the rest consisted of Fe, V and Zr. No specific fractographic features could be found in the nearest vicinity of TiN inclusions. The average dimension of TiN inclusions can be characterized by the value $\sqrt{area}$ = 12 ± 5 μm (14 measurements).

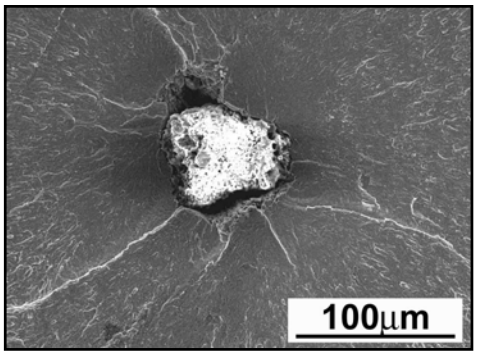

Figure 4. Large aluminium oxide inclusion at the fatigue crack origin. Tension-compression test.

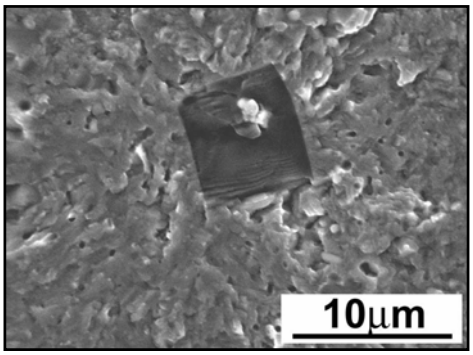

Figure 5. TiN inclusion at the fatigue crack origin. Tension-compression test.

Discussion

The finding of the absence of a clear step on the S-N curve determined in tension-compression, Fig.3a, and simultaneously the pronounced plateau on the S-N curve determined using rotating bending fatigue system supports strongly the suggestion proposed in [22] and [10] that the two-stage curve is related to the specific loading conditions under rotating bending. Rotating bending, contrary to the uniaxial tension-compression tests, is characteristic by a stress gradient. Obviously, the internal crack initiation in the case of rotating bending can be expected in the area near to the specimen surface. Results of determination of distribution of inclusions resulting in final fatigue fracture in dependence on the relative depth h/R below the surface are shown in Fig.6. R is the specimen radius. In the case of rotating bending all fractures were initiated at inclusions in the surface layer of the thickness of 0.1. On the other hand, in the case of tension-compression loading the distribution of fatigue crack origins on the specimen cross-sections is more homogeneous and internal crack initiation was observed up the relative depth of 0.5.

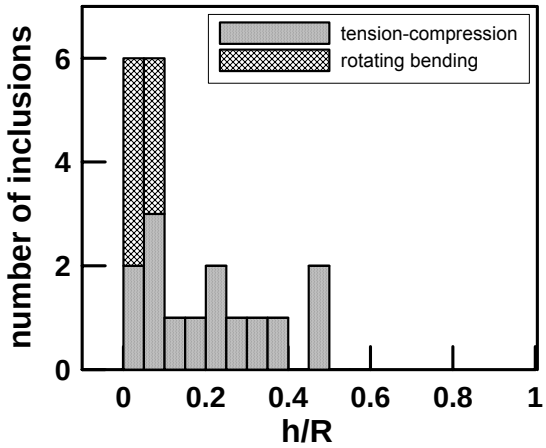

Figure 6. Distribution of inclusions resulting in final fatigue fracture in dependence on the relative depth.

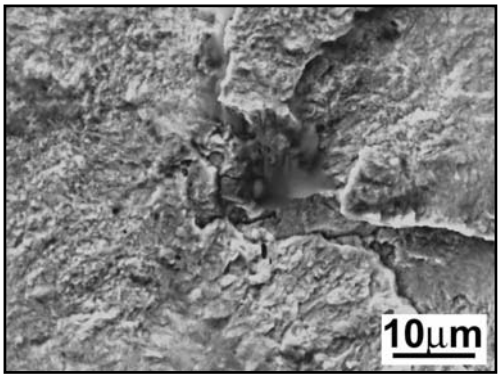

Figure 7. Internal crack initiation with traces of a dropped off TiN inclusion.

The large scatter of experimental lifetime data is a typical feature for all materials where fatigue cracks are initiated at inclusions. There is generally no good correlation between the stress amplitude and the number of cycles to fracture, Fig. 3, in the case of bearing steels. The same effect has been observed by other researches, e.g. [4, 7, 9], although high-quality material, free from nonmetallic inclusions or other stress raisers, is a primary requirement to produce bearing steels with extended fatigue life [24]. The reason of scatter consists in the fact, that the lifetime of a given specimen in the high-cycle region is determined by the particular defect having the highest stress concentration. It has been shown by Murakami et al. that the scatter of lifetime data can be reduced taking into account the effective size of inclusions and the size of the optically dark area [9]. Furuya et al. [25] reported similar results for JIS SNCM439 steel. Indeed, the presence of inclusions remains the most decisive factor influencing the fatigue behaviour of high strength bearing steels. According to our observation the TiN inclusions are mainly responsible for fatigue fracture in high-cycle and ultra-high cycle region. Their evidence on the fracture surfaces in the centre of fish eyes is often difficult; the inclusions may be fallen off or damaged, Fig. 7.

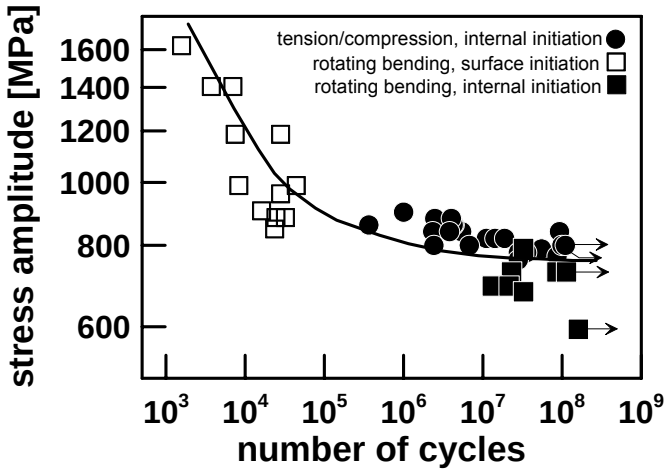

Figure 8. S-N curve based on tension-compression and corrected rotating bending data.

Experimental data from tension-compression tests together with rotating bending ones corrected in terms of the stress amplitude, which corresponds to the depth of the particular inclusion below the surface, are shown in Fig. 8. The correction shifts the stress amplitude towards lower values. The corrections can be as high as 100 MPa. It can be seen that all data can be described by one continuously decreasing curve.

An attempt to apply the Murakami's treatment [9] taking into account the inclusion size did not result in our case into a set of lifetime data having convincingly lower scatter. This correction appears to help for large aluminium oxide inclusions (which has been observed very scarcely), but for small TiN inclusions the correction does not help substantially. Large aluminium oxide inclusions have usually a spherical shape, contrary to the TiN inclusions having a plate form. Their stress concentration effect is, indeed, substantially different of that of spherical defects.

Conclusions

1. The shape of the S-N curve of bearing steel according to the Czech Standard ČSN 41 4109 depends on the loading mode. Experimental lifetime data determined in tension-compression can be best fitted by a continuously decreasing curve up to the ultra-high-cycle region. Rotating bending data exhibit a two-step shape.
2. Rotating bending data corrected in terms of the stress amplitude corresponding to the location of internal crack initiation correspond to the S-N data determined in tension-compression. The two-step appearance of the S-N curve is a consequence of the loading type and is not related to the material itself.
3. Fatigue fractures in high- and ultra-high-cycle region were initiated in material interior at inclusions predominantly of TiN type.

Acknowledgments

This research was supported by the Academy of Sciences of the Czech Republic by the grant AV0Z20410507. This support is gratefully acknowledged.

References

1. Bathias, C. and Paris, P. C., "Gigacycle Fatigue in Mechanical Practice", M. Dekker, N. York, (2005).
2. Rules for Construction of Nuclear Facility Components. ASME Boiler and Pressure Vessel Code, III Division 1, Addenda 2003.
3. Naito, T., Ueda, H. and Kikuchi, M., "Fatigue Behavior of Carburized Steel with Internal Oxides and Nonmartensitic Microstructure near the Surface", Met. Trans. **15A**, 1431-1436 (1984).

4. Bathias, C., “There is no Infinite Fatigue Life in Metallic Materials”, Fatigue Fract. Engng Mater. Struct. **22**, 559-565 (1999).
5. Nishijima, S. and Kanazawa, K.,”Stepwise S-N Curve and Fish-Eye Failure in Gigacycle Fatigue”, Fatigue Fract. Engng Mater. Struct., **22**, 601-607 (1999).
6. Sakai, T., Sato, Y. and Oguma, N. “Characteristic S-N Properties of High-Carbon-Chromium-Bearing Steel under Axial Loading in Long-Life Fatigue”, Fatigue Fract. Engng Mater. Struct., **25**, 765-773 (2002).
7. Wang, Q. Y., Baudry, G., Bathias, C. and Berard, J Y., “Subsurface Crack Initiation due to Ultra-High Cycle Fatigue”, Proc. EUROMAT 2000, Miannay, D. et al eds., Elsevier 2000, 1083-1088 (2000).
8. Tanaka, K. and Akiniwa, Y., “Fatigue Crack Propagation Behaviour Derived from S-N Data in Very High Cycle Regime”, Fatigue Fract. Engng Mater. Struct., **25**, 775-784 (2002).
9. Murakami, Y., Nomoto, T. and Ueda, T., “Factors Influencing the Mechanism of Superlong Fatigue Failure in Steels”, Fatigue Fract. Engng Mater. Struct. **22**, 581-590 (1999).
10. Murakami, Y., Yokoyama, N. N. and Nagata, J. “Mechanism of Fatigue in Ultralong Life Regime”, Fatigue Fract. Engng Mater. Struct. **25**, 735-746 (2002).
11. Miller, K. J. and O’Donnell, W. J., “The Fatigue Limit and its Elimination”, Fatigue Fract. Engng Mater. Struct. **22**, 545-557 (1999).
12. Mughrabi, H., “On the Life-Controlling Microstructural Fatigue Mechanisms in Ductile Metals and Alloys in the Gigacycle Regime”, Fatigue Fract. Engng Mater. Struct. **22**, 633-641 (1999).
13. Mughrabi, H., “Specific Features and Mechanisms of Fatigue in the Ultrahigh Cycle Regime”, Keynote lecture, Third Int. Conf. on Very High Cycle Fatigue, Ritsumeikan University, Japan (2004).
14. Shiozawa, K., Lu, L. and Ishihara, S., “S-N Curve Characteristics and Subsurface Crack Initiation Behaviour in Ultra-Long Life Fatigue of High Carbon-Chromium Bearing Steel”, Fatigue Fract. Engng Mater. Struct. **24**, 781-790 (2001).
15. Shiozawa, K. and Lu, L., “Very High-Cycle Fatigue Behaviour of Shot-Peened High-Carbon-Chromium Bearing Steel”, Fatigue Fract. Engng Mater. Struct. **25**, 813-822 (2002).
16. Ochi, Y., Matsumura, T., Masaki, K. and Yoshida, S., “High Cycle Rotating Bending Fatigue Property in Very Long Life Regime of High Strength Steels”, Proc. Int. Conf. on Fatigue in the Very High Cycle Regime, Stanzl-Tschegg, S. and Mayer, H. eds., BOKU Vienna 2001, 81-88 (2001).
17. Ueno, A. and Kishimoto, H., “Long Life Fatigue Behavior of SUJ2 Bearing Steel and FRASTA Analysis for ODA Nucleation Mechanism” ibid. 111-117.
18. Nakajima, M., Tokaji, K., Itoga, H. and Ko, H-N., “Effect of Work-Hardened Layer and Humidity on Step-Wise S-N Curve in a High Strength Steel”, ibid. 181-188.
19. Sugeta, A., Uematsu, Y. and Jono, M., “An Effect of Load Variation on High-Cycle Fatigue Behavior of SUJ2 Steels”, ibid. 325-332.
20. Collini, L., “Fatigue Life of 100Cr6 Martensitic Bearing Steel in Very High Cycle Regime”, In Proceedings of the 3rd Youth Symposium on Experimental Solid Mechanics, May 2004, Porretta Terme (Italy), 73-74, (2004).
21. Sakai, T., Takeda, M., Shiozawa, K., Ochi, Y., Nakajima, M., Nakamura, T. and Oguma, N., “Experimental Evidence of Duplex S-N Characteristics in Wide Life Region for High Strength Steels”, In: Proc. of 7th Int. Fatigue Congress, Fatigue ’99. EMAS, Higher Education Press, Beijing 1999, 573-578 (1999).
22. Marines, I., Dominguez, G., Baudry, B., Vittori, J.-F., Rathery, S., Doucet, J.-P. and Bathias, C., “Ultrasonic Fatigue Tests on Bearing Steel AISI-SAE 52100 at Frequency of 20 and 30 kHz”, Int. J. of Fatigue **25**, 1037 - 1046 (2003).
23. Q. Y. Wang, C. Bathias, N. Kawagoishi and Q. Chen, “Effect of Inclusion on Subsurface Crack Initiation and Gigacycle Fatigue Strength”, Int. J. of Fatigue 24, 1269 - 1274 (2002).
24. C. Moyer, In: Fatigue and Fracture, ASM Handbook Vol. 19, ASM Int. Ohio, Materials Park, 355 – 362 (1996).